

The Uncorrelated Universe: Statistical Anisotropy and the Vanishing Angular Correlation Function in WMAP Years 1-3

Craig J. Copi¹, Dragan Huterer², Dominik J. Schwarz³, and Glenn D. Starkman^{1,4}

¹ *Department of Physics, Case Western Reserve University, Cleveland, OH 44106-7079*

² *Kavli Institute for Cosmological Physics and Department of Astronomy and Astrophysics, University of Chicago, Chicago, IL 60637*

³ *Fakultät für Physik, Universität Bielefeld, Postfach 100131, 33501 Bielefeld, Germany and*

⁴ *Beecroft Institute for Particle Astrophysics and Cosmology, Astrophysics, University of Oxford, UK*

The large-angle (low- ℓ) correlations of the Cosmic Microwave Background (CMB) as reported by the Wilkinson Microwave Anisotropy Probe (WMAP) after their first year of observations exhibited statistically significant anomalies compared to the predictions of the standard inflationary big-bang model. We suggested then that these implied the presence of a solar system foreground, a systematic correlated with solar system geometry, or both. We re-examine these anomalies for the data from the first three years of WMAP's operation. We show that, despite the identification by the WMAP team of a systematic correlated with the equinoxes and the ecliptic, the anomalies in the first-year Internal Linear Combination (ILC) map persist in the three-year ILC map, in all-but-one case at similar statistical significance. The three-year ILC quadrupole and octopole therefore remain inconsistent with statistical isotropy – they are correlated with each other (99.6%C.L.), and there are statistically significant correlations with local geometry, especially that of the solar system. The angular two-point correlation function at scales > 60 degrees in the regions outside the (kp0) galactic cut, where it is most reliably determined, is approximately zero in all wavebands and is even more discrepant with the best fit Λ CDM inflationary model than in the first-year data – 99.97%C.L. for the new ILC map. The full-sky ILC map, on the other hand, has a non-vanishing angular two-point correlation function, apparently driven by the region inside the cut, but which does not agree better with Λ CDM. The role of the newly identified low- ℓ systematics is more puzzling than reassuring.

PACS numbers: 98.80.-k

I. INTRODUCTION AND RESULTS

Approximately three years ago, the Wilkinson Microwave Anisotropy Probe (WMAP) team reported [1–5] the results of its preliminary analysis of the satellite's first year of operation. While the data is regarded as a dramatic confirmation of standard inflationary cosmology, anomalies exist.

Among the unexpected first-year results, there is a natural division into several classes: (1) a lack of large angle correlations [1], and violations of statistical isotropy in the associated multipoles — $\ell = 2$ and 3 [6, 7]; plus weaker evidence for a violation of statistical isotropy at $\ell = 6$ and 7 [8]; (2) statistically anomalous values for the angular power spectrum, C_ℓ in at least three ℓ bins: a trough at $\ell = 22(20 - 24)$, a peak at $\ell = 40(37 - 44)$, and a trough at $\ell = 210(201 - 220)$ [3]; (3) hemispheric asymmetries in the angular power spectrum over a wide range of ℓ [9]; (4) unexpectedly high cross-correlation between temperature and E-mode polarization (TE) at low ℓ [1], interpreted by the WMAP team as evidence for a large optical depth and thus for very early star formation [5]; and a discrepancy between the observed TE angular power at the largest scales and the best fit concordance model [10].

In this paper, we focus on the large angle anomalies of the microwave background as measured in the satellite's first three years of operation, and recently reported by the WMAP team. In particular, we look at

how the full three-year WMAP results [11–14] (hereafter WMAP123) are similar to or different from those obtained from the analysis of first-year data (WMAP1). Given the high signal-to-noise of the first-year WMAP maps over a large number of well distributed pixels, in the absence of newly-identified systematic effects, one would not expect significant changes in the low- ℓ multipoles between the one-year and three-year data. The recent detailed analysis of [15] quantified this expectation, but suggested that the quadrupole, being anomalously low, is the least robust of the low multipoles.

In Section II we repeat our previous analysis of the CMB data using the multipole vector framework [7, 16]. In Section III we recall the lack of angular correlation at large angles, as measured by COBE-DMR [17] and confirmed by WMAP1 [5], but not investigated in the recent analysis of the WMAP team. We therefore include our own preliminary analysis of the angular two-point correlation function in this paper. We discuss the consequences of our findings in Section IV.

For the multipole vector analysis we compute the quadrupole and octopole multipole vectors and associated area vectors [18] of the WMAP123 full sky map (ILC123) [19], and compare them with those derived [7, 16] from three full sky maps based on WMAP1 data — WMAP's own ILC1 map [20]; Tegmark, de Oliveira-Costa and Hamilton's (TOH1) map [21]; and the Lagrange multiplier Internal Linear Combinations map (LILC1) [22]. We look at the correlations among the quadrupole and octopole area vectors, and con-

firm that in the ILC123 these are anomalously aligned ($\gtrsim 99.5\%$ C.L.), as found [7, 16] in the ILC1, TOH1 and LILC1 (99.4% C.L.; confirming and strengthening earlier results in [6]). We confirm that, as for the first-year maps, these alignments are strengthened by proper removal of the Doppler contribution to the quadrupole [7].

Having established the mutual alignment of the four planes defined by the quadrupole and octopole, we recall that in the WMAP1 maps it was found [7, 16] that these planes were aligned not just among themselves, but also with several physical directions or planes. As in the previous work we study these alignments both with and without accepting the internal correlations between the quadrupole and octopole as given. We find that the alignments generally retain the same significance as in the first-year all-sky maps. Only the alignment between the ecliptic plane and the quadrupole and octopole planes, especially given the latter’s internal correlations, is noticeably weakened. Meanwhile, there persist further correlations of the ecliptic and the quadrupole-plus-octopole, which rely strongly on the alignment of the quadrupole and octopole planes with the ecliptic.

Finally we also examine the map of the combined quadrupole and octopole and observe that, as for WMAP1, the ecliptic plane traces a zero of the map over approximately one-third of the sky, and separates the two strongest extrema in the southern ecliptic hemisphere from the two weakest extrema in the northern hemisphere.

Given the evidence for the lack of statistical isotropy on large scales we provide a careful description of the definition of the angular two-point correlation function means and connections between different possible definitions of this function. Our analysis shows that the angular two-point correlation function is strikingly deficient at large angles – in fact, the deficit of power is even more significant in the new data than in the first year data (99.97% C.L. for the ILC123 in the region outside the kp0 galaxy mask). Moreover, we find that the quadrupole and octopole power computed directly from the cut-sky maps are inconsistent with the quadrupole and octopole computed from the maximum likelihood estimators (the latter then being used for all cosmological analyses). In the conclusions section we discuss the implications of these findings.

II. MULTIPOLE VECTORS

Several large-angle anomalies or putative anomalies in the CMB data have been pointed out and discussed extensively in the literature [6, 7, 9, 10, 16, 18, 23–35]. Similarly, several novel methods proposed to study the statistical isotropy or Gaussianity of the CMB have also been introduced and discussed in the literature [36–39]. Here we focus on our previous studies [7, 16], namely the alignment of the quadrupole and octopole with each other and with physical directions on the sky as revealed

by the multipole vector formalism [18].

The ℓ -th multipole of the CMB, T_ℓ , can, instead of being expanded in spherical harmonics, be written uniquely [18, 40, 41] in terms of a scalar $A^{(\ell)}$ which depends only on the total power in this multipole and ℓ unit vectors $\{\hat{v}^{(\ell,i)} | i = 1, \dots, \ell\}$. These “multipole vectors” encode all the information about the phase relationships of the $a_{\ell m}$. Heuristically,

$$T_\ell \approx A^{(\ell)} \prod_{i=1}^{\ell} (\hat{v}^{(\ell,i)} \cdot \hat{e}), \quad (1)$$

where $\hat{v}^{(\ell,i)}$ is the i^{th} multipole vector of the ℓ^{th} multipole. (In fact the right hand side contains terms with “angular momentum” $\ell-2, \ell-4, \dots$. These are subtracted by taking the appropriate traceless symmetric combination, as described in [7, 18] and [16].) Note that the signs of all the vectors can be absorbed into the sign of $A^{(\ell)}$, so one is free to choose the hemisphere of each vector. Unless otherwise noted, we will choose the north galactic hemisphere when quoting the co-ordinates of the multipole vectors, but in plots we will show the vector in both hemispheres.

A. Multipole Vectors: WMAP1 vs. WMAP123

Multipole vectors are best calculated on cleaned full sky maps. The ILC1, TOH1, and LILC1 are all minimum-variance maps obtained from WMAP’s single-frequency maps, but differ in the detailed implementation of this idea. These full-sky maps may have residual foreground contamination, probably mainly due to imperfect subtraction of the Galactic signal. They also have complicated noise properties [2] that make them less than ideal for cosmological tests. While one can, in principle, straightforwardly compute the true (full-sky) multipole vectors from the single-frequency maps with a sky cut, a cut larger than a few degrees across will introduce significant uncertainty in the reconstructed full-sky multipole vectors and consequently in any statistics that use them (see Section 7 and Figure 7 of [16]).

The multipole vectors for $\ell = 2$ and 3 for the Doppler-quadrupole-corrected ILC1, TOH1, LILC1 and ILC123 maps are given in Table I and plotted in Figure 1. It is important that the Doppler contribution to the quadrupole, inferred from the measured dipole, has been removed before computing the multipole vectors. Although the Doppler-induced piece of the quadrupole is a small part of the total power, as shown in [7] and [16], failure to properly correct the quadrupole for the Doppler contribution results in reduced significance for the quadrupole-octopole correlations in all full sky maps. Freeman *et al.* [8] have suggested that both the lack of low- ℓ power and certain reported violations of statistical isotropy (in particular any north-south asymmetry) reported in cut-sky analysis could be due to the use of a wrong value for the dipole. However, uncertainty in the

TABLE I: Multipole vectors, $\hat{v}^{(\ell,i)}$, and area vectors $\vec{w}^{(\ell;i,j)}$, for the quadrupole and octopole in Galactic coordinates (l, b) . (Magnitudes are also given for the area vectors.) All vectors are given for the ILC123, ILC1, TOH1, and LILC1 maps after correcting for the kinetic quadrupole.

Vector	l	b	Magnitude	Vector	l	b	Magnitude
ILC123				ILC1			
$\hat{v}^{(2,1)}$	119° 6	10° 8	—	$\hat{v}^{(2,1)}$	115° 2	23° 6	—
$\hat{v}^{(2,2)}$	5° 9	19° 6	—	$\hat{v}^{(2,2)}$	19° 5	8° 6	—
$\vec{w}^{(2;1,2)}$	−128° 3	63° 0	0.951	$\vec{w}^{(2;1,2)}$	−88° 9	64° 4	0.999
$\hat{v}^{(3,1)}$	93° 8	39° 5	—	$\hat{v}^{(3,1)}$	95° 3	37° 0	—
$\hat{v}^{(3,2)}$	23° 9	8° 3	—	$\hat{v}^{(3,2)}$	21° 7	9° 4	—
$\hat{v}^{(3,3)}$	−46° 3	11° 7	—	$\hat{v}^{(3,3)}$	−47° 0	10° 7	—
$\vec{w}^{(3;1,2)}$	−76° 1	50° 0	0.936	$\vec{w}^{(3;1,2)}$	−80° 9	52° 9	0.947
$\vec{w}^{(3;2,3)}$	154° 9	77° 5	0.934	$\vec{w}^{(3;2,3)}$	161° 7	77° 8	0.924
$\vec{w}^{(3;3,1)}$	−143° 9	32° 9	0.892	$\vec{w}^{(3;3,1)}$	−144° 3	33° 9	0.861
TOH1				LILC1			
$\hat{v}^{(2,1)}$	118° 9	25° 1	—	$\hat{v}^{(2,1)}$	125° 8	16° 4	—
$\hat{v}^{(2,2)}$	11° 2	16° 6	—	$\hat{v}^{(2,2)}$	5° 9	17° 6	—
$\vec{w}^{(2;1,2)}$	−105° 7	56° 6	0.990	$\vec{w}^{(2;1,2)}$	−115° 3	58° 5	0.929
$\hat{v}^{(3,1)}$	86° 9	39° 3	—	$\hat{v}^{(3,1)}$	89° 2	37° 7	—
$\hat{v}^{(3,2)}$	22° 6	9° 2	—	$\hat{v}^{(3,2)}$	23° 8	9° 7	—
$\hat{v}^{(3,3)}$	−44° 9	8° 2	—	$\hat{v}^{(3,3)}$	−47° 3	10° 6	—
$\vec{w}^{(3;1,2)}$	−78.4° 6	49° 8	0.902	$\vec{w}^{(3;1,2)}$	−78° 6	51° 7	0.904
$\vec{w}^{(3;2,3)}$	173° 8	79° 5	0.918	$\vec{w}^{(3;2,3)}$	164° 5	77° 6	0.939
$\vec{w}^{(3;3,1)}$	−141° 6	38° 9	0.907	$\vec{w}^{(3;3,1)}$	−145° 4	36° 8	0.892

dipole seems not to significantly affect the correlations in quadrupole and octopole multipole vectors discussed here, as in the full-sky maps the identification of residual dipoles can be done uniquely.

We have found that the area vectors

$$\vec{w}^{(\ell;i,j)} \equiv \hat{v}^{(\ell,i)} \times \hat{v}^{(\ell,j)}. \quad (2)$$

are often more useful than the multipole vectors themselves for statistical comparison. As discussed in [16], under certain circumstances relevant to the observed quadrupole and octopole, these are closely related to the maximum-angular-momentum-dispersion-axes of [6]. They are also related to the Land and Magueijo triad [33], at least for the quadrupole, for which that triad is uniquely defined. The area vectors for ILC123 are also to be found in Table I.

As expected, the octopole multipole vectors, and consequently the octopole area vectors, are largely unchanged from ILC1 to ILC123. Somewhat unexpectedly (although see [15]) the quadrupole vectors *have* changed. This can all be seen quite clearly in Figure 1. To quantify the changes in multipole vectors we have computed the five dot products between the corresponding year 1 and year 123 quadrupole and octopole multipole vectors

$$d^{(\ell,i)} \equiv \hat{v}_{\text{ILC1}}^{(\ell,i)} \cdot \hat{v}_{\text{ILC123}}^{(\ell,i)}. \quad (3)$$

Similarly, to quantify the changes in area vectors, we have computed the dot products between the old and new area

vectors

$$\Delta^{(\ell;i,j)} \equiv \frac{\vec{w}_{\text{ILC1}}^{(\ell;i,j)} \cdot \vec{w}_{\text{ILC123}}^{(\ell;i,j)}}{|\vec{w}_{\text{ILC1}}^{(\ell;i,j)}| |\vec{w}_{\text{ILC123}}^{(\ell;i,j)}|} \quad (4)$$

and also the ratios of lengths between year 1 and year 123 corresponding area vectors

$$r^{(\ell;i,j)} \equiv \frac{|\vec{w}_{\text{ILC1}}^{(\ell;i,j)}|}{|\vec{w}_{\text{ILC123}}^{(\ell;i,j)}|}. \quad (5)$$

These are all found in Table II, together with comparison values for the dot products of vectors in the ILC1 and TOH1 maps. In the case of the octopole the change from ILC1 to ILC123 is comparable to the differences among different full sky maps constructed with the WMAP1 data but the change from ILC1 to ILC123 is considerably larger for the quadrupole.

The change in the ILC quadrupole is partly due to WMAP's identification of a systematic effect in the model of the radiometer gain as a function of time [11] and partly due to the correction of a bias of the ILC map [12]. Let us for the convenience of the reader paraphrase the details given in [11] and [12] to explain both effects.

The radiometer gain is the voltage difference measured as a result of changing sky-temperature differences as the satellite sweeps the sky. Besides the sky temperature, the radiometer gain depends on the temperature of the optical and electronic components involved, especially the receiver box, which houses the radiometers and

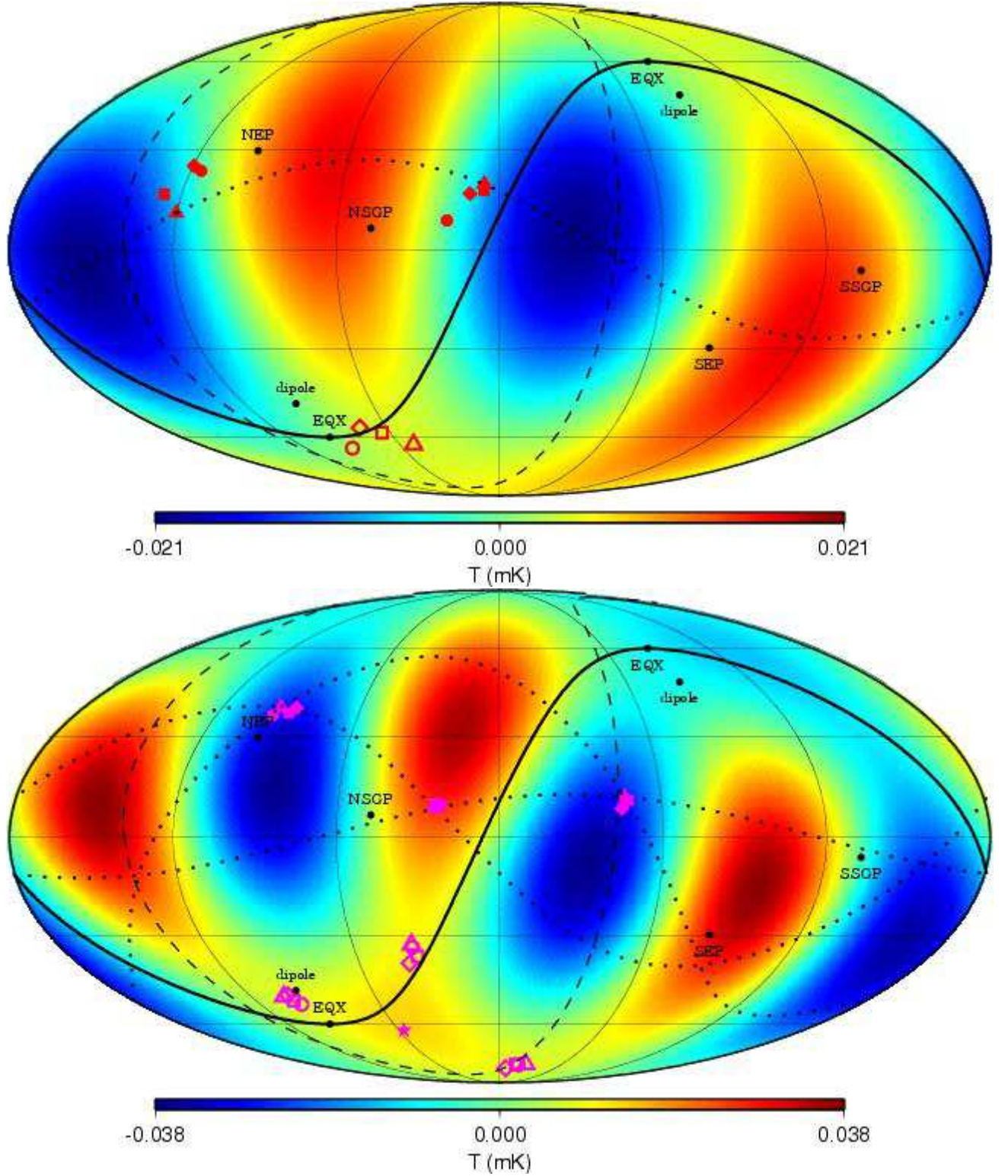


FIG. 1: The $\ell = 2$ (top panel) and $\ell = 3$ (bottom panel) multipoles from the ILC123 cleaned map, presented in Galactic coordinates, after correcting for the kinetic quadrupole. The solid line is the ecliptic plane and the dashed line is the supergalactic plane. The directions of the equinoxes (EQX), dipole due to our motion through the Universe, north and south ecliptic poles (NEP and SEP) and north and south supergalactic poles (NSGP and SSGP) are shown. The multipole vectors are plotted as the solid red symbols for $\ell = 2$ and solid magenta for $\ell = 3$ (dark and medium gray in gray scale versions) for each map, ILC1 (circles), ILC123 (triangles), TOH1 (diamonds) and LILC1 (squares). The open symbols of the same shapes are for the normal vectors for each map. The dotted lines are the great circles connecting each pair of multipole vectors for the ILC123 map. For $\ell = 3$ (bottom panel), the solid magenta (again medium gray in the gray scale version) star is the direction of the maximum angular momentum dispersion axis for the ILC123 octopole.

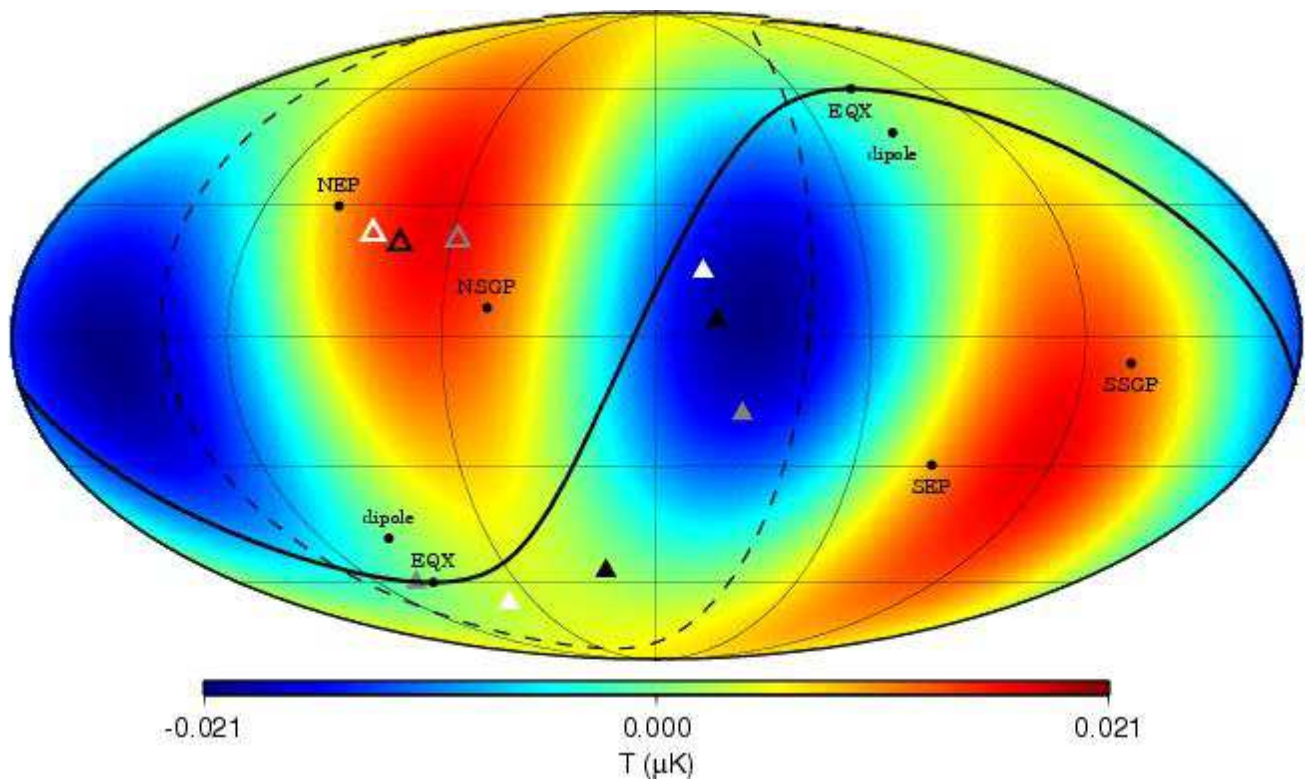


FIG. 2: The quadrupole vectors (filled triangles) and normals (open triangles) of the yr1-yr123 *difference* maps for the V band (white), W band (black) and the ILC (grey). The background shows the ILC123 quadrupole in the same coordinates as in Figs. 1 and 3.

their electronics. The satellite's temperature and with it the temperature of the receiver box changes periodically with season and shows a slight long-term increase due to the degrading of WMAP's sun shields by the Sun's UV radiation [11]. Consequently, seasonal modulation and longer-term temperature drift of the receiver box must be included in a radiometer gain model, which is needed to calibrate the sky maps. The gain model is fitted to the hourly measurement of the CMB dipole, and consequently the quality of that fit also depends on the precision to which the value and orientation of the CMB dipole are known. While in the calibration of WMAP1 the COBE/DMR dipole has been used, the WMAP123 analysis relies on the WMAP1 dipole. Having three years of data and an improved CMB dipole measurement at hand enabled the WMAP team to significantly improve the WMAP123 gain model over the WMAP1 data set. The effect of the improved gain model would be expected to be correlated with the ecliptic plane, the equinoxes (seasons) and the CMB dipole, due to the reasons given above. The seasonal effect must show up most prominently in the quadrupole (as there are four seasons). The WMAP team estimates that the residual error on the quadrupole power is $\Delta C_2 = 29 \mu K^2$.

For the synthesis of the ILC (full-sky) map an additional reported systematic correction ("galaxy bias") adds to the map a quadrupole and octopole aligned with

the galaxy to correct for the fact that a minimal variance reconstruction of the full sky tends to maximize the cancellation between the underlying signal and any foregrounds, which are dominantly galactic [12]. The WMAP team estimates that the residual error of the full-sky ILC after bias correction is $< 5 \mu K$ at larger than 10 degrees. This bias correction apparently affects the overall quadrupole power more than the correction to the gain model does, but affects the quadrupolar multipole vector structure less.

In particular, we have checked that it is the new gain model that slightly changes the orientation of the quadrupole plane (defined by $\vec{w}^{(2;1,2)}$) in the individual band maps and in the ILC map. We determined the multipole vectors of the 1yr-123yr difference full-sky maps of the V and W bands. As shown in Fig. 2, we find that the quadrupole vectors of the difference maps of the bands are quite close to the ecliptic. The associated normals are close both to the ecliptic poles, and to one of the maxima of the ILC123 quadrupole within the ILC123 quadrupole plane. (Indeed they lie between them.) Thus, the 1yr-123yr difference maps for the V and W bands show a quadrupole that is orthogonal to the ILC123 quadrupole and parallel to the ecliptic. Especially in the V band (supposed to be the least foreground contaminated band), one of the quadrupole vectors of the difference map not only lies in the ecliptic plane, but is

TABLE II: Comparisons between ILC1 and ILC123 multipole vectors and area vectors. Three quantities are tabulated: (a) dot products $d^{(\ell,i)}$ between the multipole vectors from the ILC1, $\hat{v}_{\text{ILC1}}^{(\ell,i)}$ and the corresponding vectors from the ILC123, $\hat{v}_{\text{ILC123}}^{(\ell,i)}$, for $\ell = 2$ through $\ell = 7$; (b) dot products $\Delta^{(\ell,i,j)}$ between the normalized area vectors from the ILC1, $\hat{w}_{\text{ILC1}}^{(\ell,i,j)}$ and the corresponding area vectors from the ILC123, $\hat{w}_{\text{ILC123}}^{(\ell,i,j)}$, for $\ell = 2$ and $\ell = 3$; (c) ratios $r^{(\ell,i,j)}$ between the magnitude of the area vectors from the ILC1 $|\hat{w}_{\text{ILC1}}^{(\ell,i,j)}|$ and the corresponding magnitudes $|\hat{w}_{\text{ILC123}}^{(\ell,i,j)}|$ from the ILC123, for $\ell = 2$ and $\ell = 3$. For comparison, we show in column 3 the same quantity for ILC1 versus TOH1.

Vector	ILC1-ILC123	ILC1-TOH1
$d^{(2,1)}$	0.973	0.998
$d^{(2,2)}$	0.956	0.980
$\Delta^{(2;1,2)}$	0.955	0.981
$r^{(2;1,2)}$	0.951	1.010
$d^{(3,1)}$	0.999	0.993
$d^{(3,2)}$	0.999	1.000
$d^{(3,3)}$	1.000	0.998
$\Delta^{(3;1,2)}$	0.997	0.998
$\Delta^{(3;2,3)}$	1.000	0.999
$\Delta^{(3;3,1)}$	1.000	0.995
$r^{(3;1,2)}$	0.988	1.050
$r^{(3;2,3)}$	1.010	1.006
$r^{(3;3,1)}$	1.036	0.949
$d^{(4,1)}$	0.999	0.998
$d^{(4,2)}$	0.996	0.981
$d^{(4,3)}$	0.988	0.998
$d^{(4,4)}$	0.998	0.993
$d^{(5,1)}$	0.999	0.999
$d^{(5,2)}$	0.999	1.000
$d^{(5,3)}$	1.000	0.998
$d^{(5,4)}$	1.000	0.997
$d^{(5,5)}$	1.000	0.996
$d^{(6,1)}$	0.995	0.979
$d^{(6,2)}$	0.983	0.993
$d^{(6,3)}$	0.999	0.999
$d^{(6,4)}$	0.997	0.983
$d^{(6,5)}$	0.993	0.987
$d^{(6,6)}$	1.000	0.999
$d^{(7,1)}$	0.996	0.997
$d^{(7,2)}$	0.998	0.994
$d^{(7,3)}$	1.000	0.998
$d^{(7,4)}$	0.998	0.979
$d^{(7,5)}$	1.000	1.000
$d^{(7,6)}$	0.999	0.997
$d^{(7,7)}$	1.000	0.999

also very close to the equinoxes.

The additional effect of the ILC bias correction on the quadrupole orientation can be estimated by analyzing the difference map ILC1-ILC123. Now one of the quadrupole vectors is very close to the equinoxes and the quadrupole area is close to the quadrupole areas from the V and W 1yr-123yr difference maps. Compared with the difference maps of the individual bands, the second quadrupole vector is at higher galactic latitude, which is the signature of the admixture of a galactic signal from the ILC bias correction (a galactic signal is expected to have its quadrupole vectors at high galactic latitudes [16]).

WMAP's identification of an ecliptic and equinox correlated effect in the radiometer gain is an impressive demonstration that the method of multipole vectors is very sensitive to systematic effects and/or unexpected physics — and has now proven to be a powerful tool for modern CMB data analysis.

On the other hand, we think it is quite disturbing that the signature of the systematic correction (the difference quadrupole vectors and area) seems to be anti-correlated (all the vectors are orthogonal to each other) with the supposedly cosmic signal. If both the gain model correction and the bias correction would be all that is needed to get rid of any non-cosmic signal, one would expect that the cosmic signal is uncorrelated with the correction. We think that these observations imply the presence of rather odd conspiracies between underlying signal and systematics. *We suggest that there are additional systematics or foregrounds still to be identified.*

B. Multipole Vectors: Violations of Statistical Isotropy

In [7] and [16] we pointed out a number of unusual properties of the quadrupole and octopole apparent in the WMAP1 full-sky maps (other authors have analyzed the WMAP sky using the multipole vectors, e.g. [42–47]). Here we review these properties for the ILC123 maps as illustrated in Figures 1 and 3. We refer the reader to Section 4 of [16] for further details concerning ILC1, TOH1 and LILC1.

1. The Queerness of the Quadrupole (cf. Fig. 1 top panel). The changes in the quadrupole multipole vectors are noticeable.
 - (a) The normalized quadrupole area vector $\hat{w}^{(2;1,2)}$ still lies near the ecliptic plane but has moved slightly away from the plane.
 - (b) $\hat{w}^{(2;1,2)}$ appears somewhat aligned with both the dipole and the equinoxes but has also moved away from these locations.
2. The Oddness of the Octopole (cf. Fig. 1 bottom panel). The octopole has not changed beyond expectations.

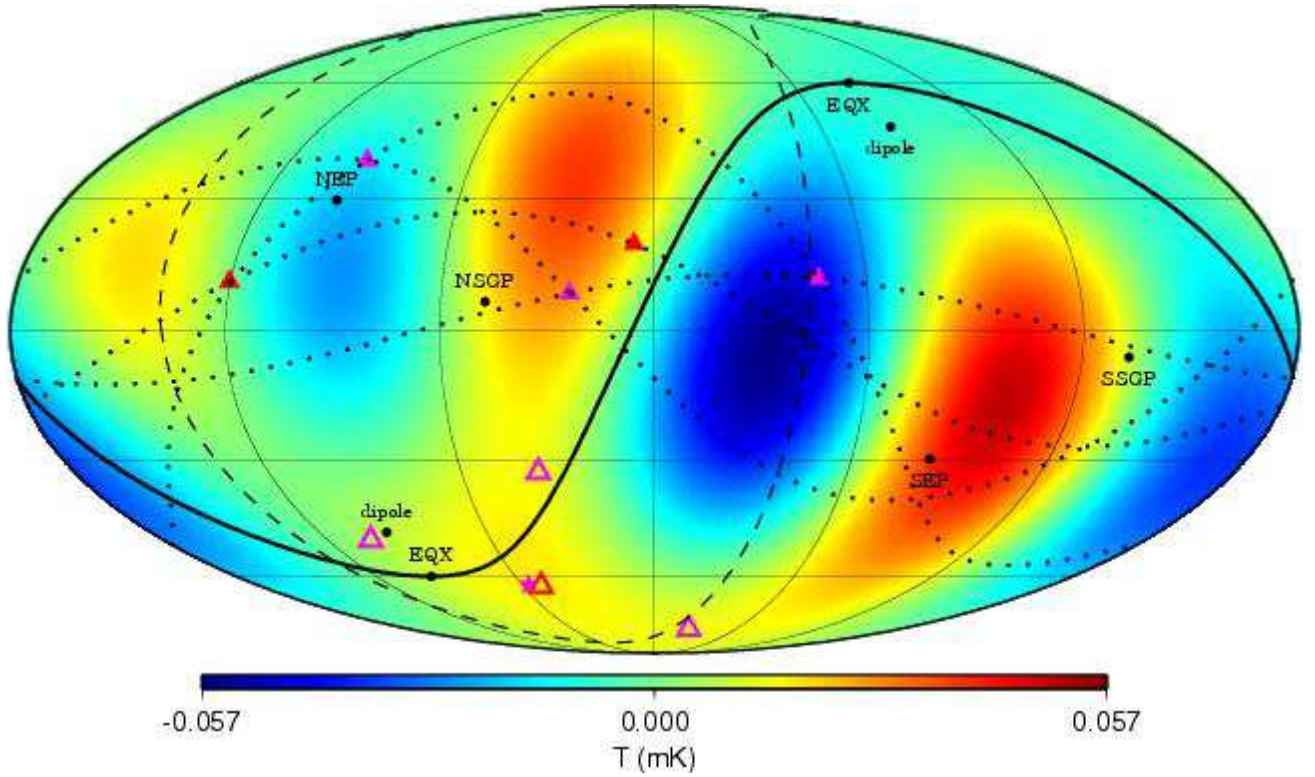


FIG. 3: The $\ell = 2 + 3$ multipoles from the ILC123 cleaned map, presented in Galactic coordinates. This is a combination of the two panels of Fig. 1 with only the multipole vectors for the ILC123 map shown for clarity. The solid line is the ecliptic plane and the dashed line is the supergalactic plane. The directions of the equinoxes (EQX), dipole due to our motion through the Universe, north and south ecliptic poles (NEP and SEP) and north and south supergalactic poles (NSGP and SSGP) are shown. The $\ell = 2$ multipole vectors are plotted as the solid red (dark gray in gray scale version) triangle and their normal is the open red (dark gray in the gray scale version) triangle. The $\ell = 3$ multipole vectors are the solid magenta (medium gray in gray scale version) triangles and their three normals are the open magenta (medium gray in the gray scale version) triangles. The dotted lines are the great circles connecting the multipole vectors for this map (one for the quadrupole vectors and three for the octopole vectors). The solid magenta (again medium gray in the gray scale version) star is the direction to the maximum angular momentum dispersion for the octopole.

- (a) Two of the normalized octopole area vectors, $\hat{w}^{(3;1,2)}$ and $\hat{w}^{(3;3,1)}$, lie near the ecliptic plane.
 - (b) The remaining normalized octopole area vector, $\hat{w}^{(3;2,3)}$, lies very near the supergalactic plane, and about 10° from the Galactic pole.
 - (c) The octopole appears somewhat planar — the three normalized octopole area vectors cluster somewhat more than expected.
3. The Remarkable Relation of the Quadrupole and Octopole (cf. Fig. 3). For the most part the relationship of the quadrupole and octopole hasn't changed.
- (a) The normalized quadrupole area vector is aligned with the normalized octopole area vectors in the sense that it lies “in the middle” of these vectors. Furthermore, it now lies very close to the octopole's maximum angular momentum dispersion direction [6].
 - (b) The ecliptic carefully traces a zero of the combined map, almost perfectly over the entire hemisphere containing the Galactic center, and relatively well over the antipodal hemisphere.
 - (c) Two of the three extrema south of the ecliptic are clearly stronger than any north of the ecliptic. The strongest of the three northern extremum is only comparable in strength to the weakest southern extremum.

The above observations are purely qualitative. Their statistical significance must be evaluated. To this end we developed several statistical tests for application to the first-year maps; we now repeat these tests for ILC123. Although we have also applied some of these tests to higher multipoles (with possibly interesting results), we defer consideration of higher multipoles to a future paper.

TABLE III: Comparison of the values of the A_i (the dot products of the quadrupole area vector with each of the three octopole area vectors). A_i and $S(A_i) \equiv (A_1 + A_2 + A_3)/3$ are tabulated for ILC1, TOH1, LILC1 and ILC123, as well as the percentile rank (out of 100) of $S(A_i)$ among a suite of 10^5 Gaussian random statistically isotropic skies. For the ILC123 map we show the results with and without the DQ-correction.

	ILC1	TOH1	LILC1	ILC123 uncorr	ILC123
A_1	0.9251	0.8509	0.7798	0.716	0.7666
A_2	0.7864	0.7829	0.7434	0.757	0.7924
A_3	0.6077	0.7616	0.7229	0.626	0.7221
$S(A_i)$	0.7731	0.7985	0.7487	0.700	0.7604
$\mathcal{P}[S(A_i)]$	0.289	0.117	0.602	1.831	0.433

1. Correlations Among Multipole Vectors

We first consider the alignment between the quadrupole area vector and the three octopole area vectors. This alignment can be measured by the magnitudes of the dot products between $\vec{w}^{(2;1,2)}$ and each of $\vec{w}^{(3;i,j)}$. We define these, according to the ordering from the largest to the smallest for the first-year full-sky maps (ILC1, TOH1, LILC1):

$$\begin{aligned} A_1 &\equiv |\vec{w}^{(2;1,2)} \cdot \vec{w}^{(3;1,2)}| \\ A_2 &\equiv |\vec{w}^{(2;1,2)} \cdot \vec{w}^{(3;2,3)}| \\ A_3 &\equiv |\vec{w}^{(2;1,2)} \cdot \vec{w}^{(3;3,1)}| \end{aligned} \quad (6)$$

A natural choice of statistic which defines an ordering relation on the three dot products is [7, 16, 43]

$$S(A_i) = \frac{1}{3} \sum_{i=1}^3 A_i. \quad (7)$$

In Table III the values of the A_i and $S(A_i)$ are shown for ILC1, TOH1, LILC1 and ILC123. As expected, the differences between ILC1 and ILC123 appear comparable to the systematic errors in making full sky maps, as measured by the differences between the ILC1, TOH1 and LILC1 values. However, in contrast to the first year maps the ILC123 obeys the ordering $A_2 > A_1 > A_3$, which is due to the fact that the area vector of the quadrupole has changed significantly.

We have compared the values of the A_i against 10^5 Monte Carlos of Gaussian random statistically isotropic skies with pixel noise (as in [18]). Of course, WMAP1 data is compared to Monte Carlo simulations with the one-year pixel noise, while for WMAP123 data we use the appropriate three-year pixel noise. The percentile rank \mathcal{P} of the $S(A_i)$ values for each of the four full sky maps among the 10^5 associated Monte Carlos is also listed in Table III. The clear inference to be drawn is that the quadrupole and octopole show a statistically significant correlation with each other in the ILC123 map, just as

they do in the WMAP first-year all-sky maps. This correlation is at the 99.6%C.L. for ILC123, within the range seen for the WMAP1 maps (99.4 – 99.9%C.L.).

Also included in Table III are the values of the A_i and the associated statistics for an ILC123 from which the Doppler contribution to the quadrupole has not been removed (ILC123 uncorr). As for WMAP123, we see that the correlation between quadrupole and octopole is significantly stronger in the properly corrected map than in the uncorrected map.

2. Correlations of area vectors with physical directions

So far we have looked only at the internal correlations between the CMB quadrupole and octopole. We have previously [7, 16] examined the correlation of the quadrupole and octopole area vectors with various physical directions, and inferred that the quadrupole and octopole are also correlated not just with each other but also with the geometry of the solar system. We now re-examine these correlations quantitatively for WMAP123.

Our measure of alignment of the area vectors with a physical direction \hat{d} is

$$S^{(4,4)}(\hat{d}) \equiv \frac{1}{4} \left(|\hat{d} \cdot \vec{w}^{(2;1,2)}| + |\hat{d} \cdot \vec{w}^{(3;1,2)}| + |\hat{d} \cdot \vec{w}^{(3;2,3)}| + |\hat{d} \cdot \vec{w}^{(3;3,1)}| \right). \quad (8)$$

In Table IV, we display the probabilities of the $S^{(4,4)}(\hat{d})$ statistic for the various WMAP1 and WMAP123 full-sky maps computed for: the ecliptic plane, the galactic poles (NGP), the supergalactic plane, the CMB dipole and the equinoxes. These directions and planes are the ones most obviously connected either to possible sources of systematics (ecliptic plane, CMB dipole and equinoxes) or to possible unanticipated foregrounds (ecliptic plane, galactic plane/pole, supergalactic plane). For the galactic poles, the dipole and the equinoxes, these probabilities are the percentage of statistically isotropic skies (among our usual suite of 10^5 Monte Carlo realizations of statistically isotropic skies) that exhibit a higher value of $S^{(4,4)}$ for that direction; for the ecliptic and supergalactic planes, they are the percentage of statistically isotropic skies (among the 10^5 realizations) that exhibit a lower value of $S^{(4,4)}$ for the axis of each plane.

From Table IV, we see that the correlations of the full sky map to the dipole, equinox and galactic poles remains essentially unchanged in the WMAP123 at 99.7%C.L., 99.8%C.L. and 99%C.L. respectively. Similarly the correlation to the supergalactic plane remains insignificant at 85%C.L. The correlation with the ecliptic has declined somewhat from 98%C.L. to 96%C.L.

In Section IIB 1 we established the correlation of the quadrupole and octopole area vectors with each other. One might therefore ask whether the observed correlations to physical directions could be mere accidents of the internal quadrupole-octopole correlations. In [16],

TABLE IV: The percentiles of $S^{(4,4)}(\hat{d})$ from 10^5 MC maps test for the alignment of known directions with the quadrupole and octopole area vectors. The ILC1, TOH1, LILC1 and ILC123 maps are studied. For the ILC123 map we show the results with and without DQ-correction.

	ILC1	TOH1	LILC1	ILC123	ILC123
	uncorr				
ecliptic	2.01	1.43	1.48	4.88	4.11
NGP	0.51	0.73	0.94	1.08	0.89
SG plane	8.9	14.4	13.4	10.8	15.3
dipole	0.110	0.045	0.214	0.489	0.269
equinox	0.055	0.031	0.167	0.328	0.194

we showed that for the first-year maps, even given the “shape” of the quadrupole and octopole – their multipole structure and mutual orientation – the additional correlations of their area vectors to the ecliptic plane were very significant. We also found that the additional correlations to the dipole and equinoxes was less significant, and the additional correlations to the galaxy and to the supergalactic plane were not statistically significant. We next revisit the issue for the ILC123.

To address this question, we compute the probability, *given* the shape of the quadrupole and octopole and their mutual alignment, that they would align to the extent they do with each direction or plane. Put another way, we find the fraction of directions/planes that are better aligned with the observed quadrupole and octopole than each of the directions and planes in question. Thus, we hold the quadrupole and octopole area vectors fixed and compute $S^{(4,4)}(\hat{d})$ both for the physical directions that may be of interest — the ecliptic poles, the Galactic poles, the supergalactic poles, the cosmological dipole and the equinoxes — and for a large number of random directions. We denote this test by $S^{(4,4)}(\hat{d}|\{\vec{w}\})$, meaning that the area vectors $\{\vec{w}\}$ are fixed to be the observed ones.

The results are shown graphically in Figure 4, which is a histogram of the values of $S^{(4,4)}(\hat{d}|\{\vec{w}\})$ for the randomly chosen directions, with the values of $S^{(4,4)}(\hat{d}|\{\vec{w}\})$ for the particular physical directions shown. The interesting shape of the histogram, including the spike, is dictated by the geometry of the particular mutual orientation of the quadrupole and octopole. Directions lying within the relatively small triangle bounded by the three octopole area vectors – which contains the quadrupole area vector – contribute to the spike. The existence of the spike is therefore a consequence of quadrupole-octopole alignment.

It is clear from Figure 4 that the additional correlations with the galaxy and with the supergalactic plane are not particularly significant. To determine the precise significance we compute for each physical direction, the fraction of random directions that yield a larger value of $S^{(4,4)}(\hat{d}|\{\vec{w}\})$. These are given in Table V.

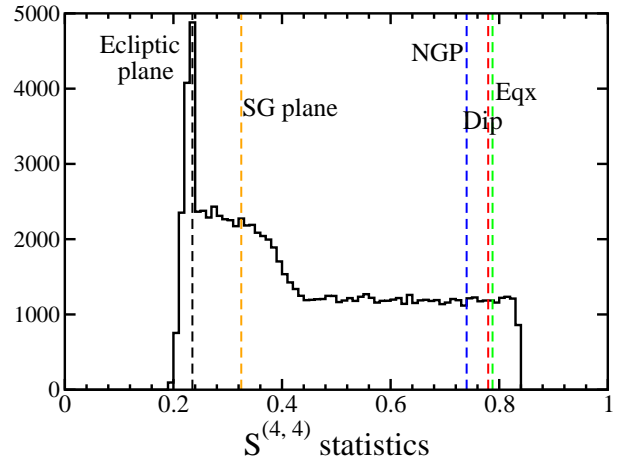


FIG. 4: Histogram of the $S^{(4,4)}(\hat{d}|\{\vec{w}\})$ statistics applied to the ILC123 map quadrupole and octopole area vectors and a fixed direction or plane on the sky, compared to 10^5 random directions. Vertical lines show the S statistics of the actual area vectors applied to the ecliptic plane, NGP, supergalactic plane, dipole and equinox directions (Table V shows the actual product percentile ranks among the random rotations for ILC1, ILC123 and TOH1). This Figure and Table V show that, *given* the relative location of the quadrupole-octopole area vectors (i.e. their mutual alignment), the dipole and equinox alignments remain unlikely at about 95% C.L., whereas the ecliptic alignment, significant at 98.3-99.8% C.L. in year 1, is only significant at the 90% C.L. in year 123. The galactic plane and supergalactic plane alignments remain not significant.

TABLE V: The percentiles of $S^{(4,4)}(\hat{d}|\{\vec{w}\})$ for the ecliptic plane, NGP, supergalactic plane, dipole and equinox axes among a comparison group of 10^5 random directions (or equivalently random planes) on the sky. The ranks are given for the ILC1, TOH1, LILC1 and ILC123 maps.

	ILC1	TOH1	LILC1	ILC123
ecliptic	1.7	1.0	0.2	10.3
NGP	90	87	88	88
SG plane	25	34	33	32
dipole	94.5	95.6	93.8	93.0
equinox	96.4	96.1	94.4	94.0

In Table V we compare the results obtained from ILC123 to those obtained from ILC1, TOH1 and LILC1. As expected, the dipolar and equinoctical values for $S^{(4,4)}(\hat{d}|\{\vec{w}\})$ remain essentially unchanged, in the 93th percentile and 94th percentile respectively among all directions. However, one should probably interpret this as just a 86% C.L. and 88% C.L. case respectively for additional correlation, because we would have found it equally surprising if they had been in the 7th or 6th percentile. The 88th percentile rank of the Galactic polar

axis similarly offers only a 76% C.L. case for additional correlation, while the supergalactic plane is clearly not additionally correlated by this measure.

Our first real surprise is that the rank $S^{(4,4)}(\hat{d}|\{\vec{w}\})$ for the (normal to the) ecliptic plane has increased from the 0.2 – 1.7 percentile range of the three WMAP1 maps to 10 percentile for the ILC123. This is because, although the altered quadrupole caused only a small increase in the actual value of $S^{(4,4)}(\hat{d}|\{\vec{w}\})$ for the dipole, the value moved from below the peak at low $S^{(4,4)}$ seen in Figure 4, into the main body of the peak. This still represents 90% C.L. evidence of additional correlation of the ecliptic, *not* 80% C.L. evidence. That is because, as we shall see in subsection II B 3, the ILC123 possesses other features strongly correlated with the ecliptic, not captured by $S^{(4,4)}(\hat{d}|\{\vec{w}\})$ (or even by the area vectors). These features would be impossible if the ecliptic $S^{(4,4)}(\hat{d}|\{\vec{w}\})$ were in the top 10 percentile of values.

On the basis of the $S^{(4,4)}(\hat{d}|\{\vec{w}\})$ statistic alone, while the additional correlation with the ecliptic is the most significant among the physical directions and planes which we have considered, it is now of only 90% C.L. significance. However, as we have suggested above, and explore below, the $S^{(4,4)}(\hat{d}|\{\vec{w}\})$ statistic captures only a part of the strange connection between the quadrupole and octopole and the ecliptic.

Some measure of caution should also be retained in dismissing any Galactic, supergalactic, dipole or equinoctic correlations just because the additional correlations are not significant. We do not know whether the correlations with those directions shown in Table IV are “accidental” consequences of the internal correlation of the quadrupole and octopole, or whether the correlation among the quadrupole and octopole area vectors is an “accidental” consequence of their correlation to a physical direction.

Finally, we caution the reader in advance that in Section III we will call into question some of the “improvements” in the ILC123 over the ILC1 that have most likely led to the unexpected decline in statistical significance of the additional correlation of the ecliptic with the quadrupole and octopole.

3. Correlations with physical directions not captured by area vectors

The statistics we have studied above do not use all the information in a multipole. The area vectors alone do not contain all this information; this is obvious for the quadrupole, and true for higher ℓ as well. Furthermore, we have considered only the dot products of the area vectors with the physical directions and planes, this again reduces the portion of information retained.

In Figure 3, we see very clearly that the ecliptic plane traces out a locus of zero of the combined quadrupole and octopole over a broad swath of the sky — neatly separating a hot spot in the northern sky from a cold spot

in the south. Indeed, it seems to separate three strong southern extrema from three weaker northern ones. This information is not contained in the $S^{(4,4)}$ statistic since it depends precisely on an extra rotational degree of freedom about an axis close to the ecliptic plane. As discussed at some length in [16], given the observed internal correlations of the quadrupole and octopole area vectors and given the correlation of those area vectors with the ecliptic, the probability of the ecliptic threading along a zero curve in the way it does is difficult to quantify exactly, but is certainly less than about 5%. Furthermore, this correlation could not occur if the area vectors were pointing toward the ecliptic poles instead of perpendicular to them. (Hence our assertion that the probability of the observed area vectors’ correlation with the ecliptic is 10%, not twice that.) This remains as true for the ILC123 maps as it was for the WMAP1 full sky maps.

4. Summary

To conclude our re-analysis of the quadrupole and octopole multipole vectors, there is still strong evidence for the quadrupole-octopole alignment and/or the alignment of the quadrupole and octopole with the ecliptic/equinox and dipole. *The data do not support the statistical isotropy of the sky at the largest angular scales.*

III. ANGULAR CORRELATION FUNCTION

The near vanishing of the two-point angular correlation function at angular separations greater than about 60 degrees has been the longest established among the anomalies in the CMB [17]. Here we compare the results from the one-year WMAP data and the three-year data. Since WMAP has not provided an analysis of the angular correlation function for the year 123 data we provide our own.

A. What is the “angular correlation function”?

There are several distinct quantities that are commonly referred to as the “two point angular correlation function” and the related “angular power spectrum”. Here we clarify how the various definitions depend on the assumptions about statistical isotropy and sky coverage of the map.

We have first

$$\tilde{C}(\hat{e}_1, \hat{e}_2) \equiv \langle T(\hat{e}_1)T(\hat{e}_2) \rangle \quad (9)$$

where $\langle \cdot \rangle$ represents an ensemble average over the temperatures $T(\hat{e}_1)$ and $T(\hat{e}_2)$ in the particular directions \hat{e}_1 and \hat{e}_2 . (The precise nature of the ensemble when we have only one universe to observe is philosophically troubling to many, but will be ignored.) If the sky were

statistically isotropic, then $\tilde{\mathcal{C}}(\hat{e}_1, \hat{e}_2)$ depends only on the angle θ between \hat{e}_1 and \hat{e}_2 . This allows us to define our first two-point angular correlation function

$$\tilde{\mathcal{C}}(\theta) \equiv \langle T(\hat{e}_1)T(\hat{e}_2) \rangle_\theta, \quad (10)$$

where $\langle \cdot \rangle_\theta$ now represents an ensemble average over the temperatures $T(\hat{e}_1)$ and $T(\hat{e}_2)$ in all pairs of directions \hat{e}_1 and \hat{e}_2 separated by the angle θ . The average $\langle \cdot \rangle_\theta$ may stand for the full sky or just a finite region of the sky. In the case of statistical isotropy any region of the sky provides the same answer, however, in the case of a statistically anisotropic sky, different regions of the sky give rise to different values of $\tilde{\mathcal{C}}(\theta)$.

We can represent $\tilde{\mathcal{C}}(\theta)$, as a sum involving the Legendre polynomials:

$$\tilde{\mathcal{C}}(\theta) = \frac{1}{4\pi} \sum_{\ell=0}^{\infty} (2\ell+1) \tilde{\mathcal{C}}_\ell P_\ell(\cos \theta), \quad (11)$$

$$\tilde{\mathcal{C}}_\ell \equiv 2\pi \int_{-1}^1 d(\cos \theta) \tilde{\mathcal{C}}(\theta) P_\ell(\cos \theta). \quad (12)$$

These $\tilde{\mathcal{C}}_\ell$ are also our first incarnation of the “angular power spectrum”.

The two point angular correlation function of equation (10) is defined as an ensemble average. By definition, we can get an unbiased estimate $\mathcal{C}(\theta)$ of $\tilde{\mathcal{C}}(\theta)$ by replacing the ensemble average (for the observed part of the sky) with an average over the observed sky, even if this is not the full sky:

$$\mathcal{C}(\theta) \equiv \overline{T(\hat{e}_1)T(\hat{e}_2)}_\theta. \quad (13)$$

This average is over all pairs of directions \hat{e}_1 and \hat{e}_2 separated by the angle θ on the actual sky. The more, independent pixels separated by an angle θ measured on the sky, the more accurate the estimate; but even if the sky is cut, the estimate is unbiased. $\mathcal{C}(\theta)$ can also be written as a sum over Legendre polynomials:

$$\mathcal{C}(\theta) = \frac{1}{4\pi} \sum_{\ell=0}^{\infty} (2\ell+1) \mathcal{C}_\ell P_\ell(\cos \theta). \quad (14)$$

An alternative to performing the average over the observed sky and then a Legendre polynomial expansion to obtain the \mathcal{C}_ℓ is to do a maximum likelihood estimate (MLE) to obtain $\mathcal{C}_\ell^{\text{MLE}}$. This has several advantages. It allows one to account for noise; for the prior probability distribution of the \mathcal{C}_ℓ (in a statistically isotropic model for the origin of fluctuations, such as inflation); and for residual galactic uncertainty [48] (by marginalizing over foreground templates). Because the MLE method gives a distribution of likelihoods as a function of the $\mathcal{C}_\ell^{\text{MLE}}$, one has a measure not just of the most likely value of each \mathcal{C}_ℓ but also of the uncertainty in that value.

Some caution is necessary in using the MLE. MLE assumes that each $T(\hat{e}_i)$ is Gaussian distributed. It also assumes statistically isotropic noise. For $\ell \leq 10$, the

WMAP team quotes [12] the peak in the likelihood distribution of $\mathcal{C}_\ell^{\text{MLE}}$ as the value of the “angular power spectrum” for that ℓ .

There is another closely related quantity, which is often called the two-point angular correlation function, but which is not identical to the ensemble average (10) except in certain circumstances. Consider the usual spherical harmonic expansion of the CMB sky

$$T(\theta, \phi) \equiv \sum_{\ell=0}^{\infty} T_\ell \equiv \sum_{\ell=0}^{\infty} \sum_{m=-\ell}^{\ell} a_{\ell m} Y_{\ell m}(\theta, \phi). \quad (15)$$

The ensemble average of the product of $a_{\ell m}$,

$$\tilde{\mathcal{C}}_{\ell m \ell' m'} \equiv \langle a_{\ell m}^* a_{\ell' m'} \rangle, \quad (16)$$

encodes the same information as $\tilde{\mathcal{C}}(\hat{e}_1, \hat{e}_2)$. The sky is statistically isotropic if and only if

$$\tilde{\mathcal{C}}_{\ell m \ell' m'} = \tilde{\mathcal{C}}_\ell \delta_{\ell \ell'} \delta_{m m'}. \quad (17)$$

In this case one can show that the angular power spectrum $\tilde{\mathcal{C}}_\ell$ are identical to the coefficients in equation (11), i.e.

$$\text{statistical isotropy} \Rightarrow (\tilde{\mathcal{C}}_\ell = \tilde{\mathcal{C}}_\ell). \quad (18)$$

Similarly, one can define a function based on the $\tilde{\mathcal{C}}_\ell$,

$$\tilde{\mathcal{C}}(\theta) \equiv \frac{1}{4\pi} \sum_{\ell=0}^{\infty} (2\ell+1) \tilde{\mathcal{C}}_\ell P_\ell(\cos \theta). \quad (19)$$

Unfortunately, we cannot compute the $\tilde{\mathcal{C}}_\ell$ from what we measure since the $\tilde{\mathcal{C}}_\ell$ are properties of the underlying ensemble of which the sky is but one realization. What we can compute are estimators of $\tilde{\mathcal{C}}_\ell$. For example, given the full sky, we could measure the $a_{\ell m}$ from the full sky and then define

$$C_\ell \equiv \frac{1}{2\ell+1} \sum_{m=-\ell}^{\ell} |a_{\ell m}|^2. \quad (20)$$

Obviously this definition is motivated by statistical isotropy, but is not restricted to that case. In the case of statistical isotropy it is an unbiased estimator of $\tilde{\mathcal{C}}_\ell$. Additionally, if Gaussianity holds, this is the best estimator with cosmic variance $\text{Var}(C_\ell) = 2\tilde{\mathcal{C}}_\ell^2/(2\ell+1)$. If Gaussianity is violated the cosmic variance may be larger.

The estimator (20) can be easily adapted to cut skies. Other similar estimators exist (and have improved performance, for example in a noisy environment [12]). If ℓ is large, C_ℓ will be a good estimate of the angular power spectrum $\tilde{\mathcal{C}}_\ell$. These C_ℓ , however precisely obtained, are often called the pseudo- \mathcal{C}_ℓ .

Finally, one can define the function based on the C_ℓ ,

$$C(\theta) \equiv \frac{1}{4\pi} \sum_{\ell=0}^{\infty} (2\ell+1) C_\ell P_\ell(\cos \theta). \quad (21)$$

TABLE VI: The four classes of pairs of quantities often called the “two-point angular correlation function” and the “angular power spectrum”. Angle brackets represent ensemble averages, an overbar represents an average over the sky or some portion thereof. LPT stands for Legendre polynomial transform, LPS for Legendre polynomial series expansion. T_i is the temperature in the i th sky pixel, $a_{\ell m}$ is the coefficient of $Y_{\ell m}$ in a spherical harmonic expansion of the temperature field on the sky. In the case of C_ℓ , the definition actually represents the canonical, but not necessarily best, estimator of \tilde{C}_ℓ , calculated from the spherical harmonic coefficients of the temperature field.

“correlation function”		“angular power-spectrum”	
symbol	definition	symbol	definition
$\tilde{C}(\theta)$	$\langle T_i T_j \rangle$	\tilde{C}_ℓ	LPS of $\tilde{C}(\theta)$
$\mathcal{C}(\theta)$	$\overline{T_i T_j}$	\mathcal{C}_ℓ	LPS of $\mathcal{C}(\theta)$
\tilde{C}_ℓ	LPT of \tilde{C}_ℓ	\tilde{C}_ℓ	$\langle a_{\ell m}^* a_{\ell m} \rangle$
$C(\theta)$	LPT of C_ℓ	C_ℓ	$\frac{1}{(2\ell+1)} \sum_m a_{\ell m} ^2$

In the case of statistical isotropy and Gaussianity the cosmic variance of the correlation function estimated from full skies becomes

$$\text{Var}(C(\theta)) = \frac{1}{8\pi^2} \sum_{\ell=0}^{\infty} (2\ell+1) \tilde{C}_\ell^2 P_\ell^2(\cos \theta). \quad (22)$$

If the C_ℓ and $\mathcal{C}(\theta)$ are inferred from a full sky measurement, then one can show that (up to pixelization errors)

$$\text{full sky} \Rightarrow (C_\ell = \mathcal{C}_\ell), \quad (23)$$

and equivalently

$$\text{full sky} \Rightarrow (C(\theta) = \mathcal{C}(\theta)). \quad (24)$$

The relationships among these quantities are summarized in Table VI.

While the temptation not to differentiate between these quantities is understandable, we would argue for a preference to reserve for $\tilde{C}(\theta)$ (and $\mathcal{C}(\theta)$) the name angular correlation function (and its estimator); and to call \tilde{C}_ℓ (and C_ℓ) the angular power spectrum (and its estimator).

In the previous Section we presented evidence that the low- ℓ sky is *not* statistically isotropic. Moreover the $a_{\ell m}$ (or the C_ℓ) are generically *not* computed over a full sky. Therefore the distinctions between \tilde{C} and \tilde{C}_ℓ , and between \mathcal{C} and C must be kept in mind when interpreting CMB results. In particular, the measurable quantities — $\mathcal{C}(\theta)$ and C_ℓ — are *not* interchangeable, but rather encode, at least in principle somewhat *different* information about the map. This means that one must check that any analysis procedure has reasonable consequences not just for the C_ℓ , but also for $\mathcal{C}(\theta)$.

Indeed, in the absence of statistical isotropy, many of the quantities to which we are accustomed are of uncertain meaning and dubious value. For example, neither

$\tilde{C}(\theta)$ nor \tilde{C}_ℓ characterizes the statistical properties of the ensemble of which the CMB is a realization. They are averages of quantities that may (partly) characterize the ensemble — $\tilde{C}(\hat{e}_1, \hat{e}_2)$ or $\tilde{C}_{\ell m \ell' m'}$ — but, in the absence of SI, these more complicated quantities cannot be meaningfully estimated with only one sky. Estimators like $\mathcal{C}(\theta)$ and C_ℓ remain of interest primarily to the extent that either the sky is almost statistically isotropic (so that $\tilde{C}(\hat{e}_1, \hat{e}_2)$ and $\tilde{C}_{\ell m \ell' m'}$ can be expanded around $\tilde{C}(\theta)$ and $\tilde{C}_\ell \delta_{\ell \ell'} \delta_{m m'}$) or the estimators ($\mathcal{C}(\theta)$ or C_ℓ) return unexpected values.

The question of approximate statistical isotropy may be worth exploring. What is certainly true, as we show below, is that $|\mathcal{C}(\theta)|$ remains unexpectedly small at large angles in WMAP123, just as it was for COBE-DMR and WMAP1. One must therefore be extremely cautious about any reconstruction method that regards the \tilde{C}_ℓ as fundamental, independent variables, while ignoring the properties of $\mathcal{C}(\theta)$.

To summarize, while CMB cosmologists have a long-standing interest in and preference for the angular power spectrum \tilde{C}_ℓ as the relevant variables for statistical analysis, given the absence of statistical isotropy for low ℓ these variables are at best flawed. Therefore one must be careful to distinguish between \tilde{C}_ℓ and \mathcal{C}_ℓ and their estimators; one must be cautious that \tilde{C}_ℓ and \mathcal{C}_ℓ may not characterize the observed microwave maps; and one must pay careful attention to the properties of $\mathcal{C}(\theta)$.

B. The measured $\mathcal{C}(\theta)$

We can readily explore $\mathcal{C}(\theta)$, the angular correlation function, since there is indeed a very large number of independently measured pixels on the WMAP sky. $\mathcal{C}(\theta)$ was first measured (at large angles) using the Cosmic Background Explorer’s Differential Microwave Radiometer (COBE-DMR) [17], and found to be anomalously small in magnitude at large angles in all COBE bands.

The WMAP team [1, 5] using their first year of data presented the “angular correlation function”, but this was obtained from the C_ℓ (and so, was actually $C(\theta)$, not $\mathcal{C}(\theta)$). WMAP did not present any angular correlation function in their third-year papers, although, as mentioned above, their “angular power spectrum” at low ℓ were actually maximum likelihood estimates of C_ℓ , i.e. the coefficients of a Legendre polynomial series expansion of a MLE of $\mathcal{C}(\theta)$.

In Figure 5 we show $\mathcal{C}(\theta) \equiv \overline{T(\hat{e}_1)T(\hat{e}_2)}_\theta$ (computed in pixel space) for the Q, V and W band maps masked with the kp0 mask. (See [1] for a discussion of the various galactic masks.) The K and Ka bands have a large and obvious galactic contamination even after applying the kp0 mask, and we do not use them. Also shown are the correlation function for the ILC map with and without the mask, and the Legendre polynomial series of the quoted maximum likelihood estimates of C_ℓ , i.e. $\mathcal{C}^{\text{MLE}}(\theta)$. Finally, we show $\tilde{C}(\theta) = \tilde{C}(\theta)$ for the best fit

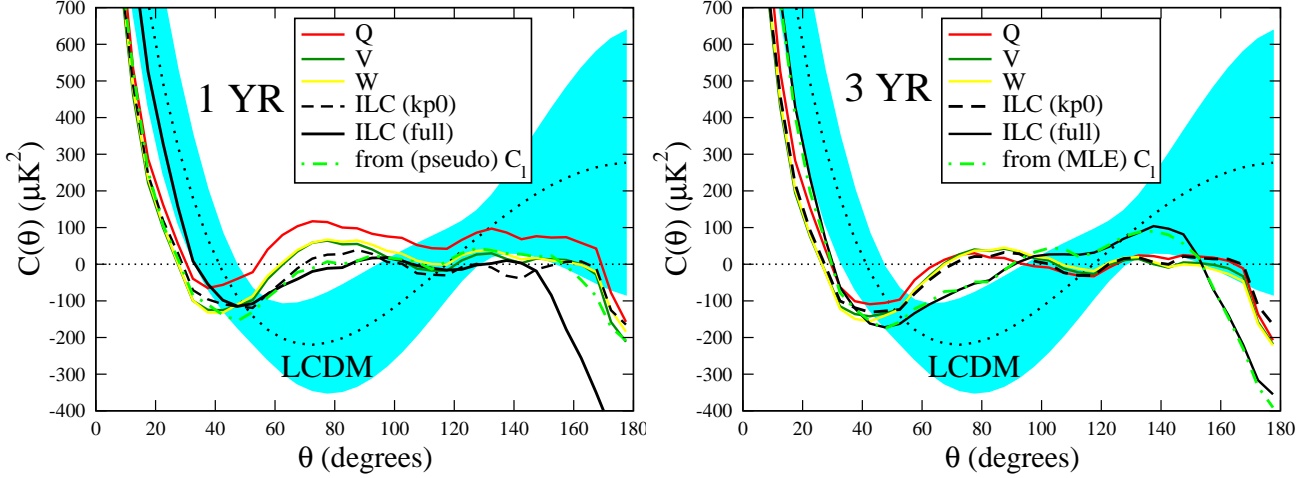


FIG. 5: Two point angular correlation function, $\mathcal{C}(\theta) \equiv \overline{T(\hat{e}_1)T(\hat{e}_2)}_\theta$ computed in pixel space, for three different bands masked with the kp0 mask. Also shown is the correlation function for the ILC map with and without the mask, and the value expected for a statistically isotropic sky with best-fit Λ CDM cosmology together with 68% error bars. Left panel: year 1 results. Right panel: year 123 results. Even by eye, it is apparent that masked year 123 maps have $\mathcal{C}(\theta)$ that is consistent with zero at $\theta \gtrsim 60$ deg, even more so than in year 1 maps. We also show the $\mathcal{C}(\theta)$ computed from the “official” published C_ℓ , which (at $\ell < 10$) are the pseudo- C_ℓ in year 1, the and MLE C_ℓ in year 123. Clearly, the MLE-based C_ℓ , as well as $\mathcal{C}(\theta)$ computed from the full-sky ILC maps, are in significant disagreement with the angular correlation function computed from cut-sky maps.

Λ CDM model of the three-year WMAP, and a blue band around that showing the range of $\mathcal{C}(\theta)$ that one would extract from a full sky, given cosmic variance. The left panel shows the year 1 results, while the right panel shows year 123 results.

First of all, we see that the different bands and the cut-sky ILC map are all in excellent agreement with each other for year 1 and year 123 separately, perhaps with an exception of the year 1 Q band map. In each case the magnitude of $\mathcal{C}(\theta)$ is very small above 60 degrees and below 170 degrees; above 170 degrees there is a peculiar slight anti-correlation while the model predicts a large positive correlation. Moreover, even by eye it is apparent that year 123 maps have $\mathcal{C}(\theta)$ that is nearly vanishing at $60 \lesssim \theta \lesssim 170$ deg even more precisely than in year 1 maps. Finally, the full-sky $\mathcal{C}(\theta)$ from the ILC maps is in agreement with i.e. $\mathcal{C}^{\text{MLE}}(\theta)$, but in significant disagreement with the cut-sky value.

We now compare the smallness of $\mathcal{C}(\theta)$ to that expected in simulated maps. We use the statistic proposed by WMAP [5] in their first-year papers that quantifies the lack of power at $\theta > 60$ degrees

$$S_{1/2} \equiv \int_{-1}^{1/2} [\mathcal{C}(\theta)]^2 d(\cos \theta). \quad (25)$$

The WMAP team computed $S_{1/2}$ for the original ILC1 and found that only 0.15% of the elements in their Markov chain of Λ CDM model CMB skies had lower values of $S_{1/2}$ than the true sky. In addition we define the

statistic

$$S_{\text{full}} \equiv \int_{-1}^1 [\mathcal{C}(\theta)]^2 d(\cos \theta), \quad (26)$$

which quantifies the amount of power squared on *all* angular scales.

In Table VII we give the value of $S_{1/2}$ for the one-year and three-year band maps, for ILC1 and ILC123, and for the best fit Λ CDM model. The values of $S_{1/2}$ and S_{full} are very low relative to what the Λ CDM isotropic cosmology predicts and are noticeably lower in the year 123 maps than in the year 1 maps.

To quantify the probabilities of our statistics, we perform comparison with 20,000 Gaussian random, isotropic realizations of the skies consistent with models favored by the WMAP data. The angular power spectrum from *each* simulated sky is generated as follows:

1. pick a model (in order of the highest weight) from WMAP’s publicly available Markov chains;
2. generate the angular power spectrum in multipole space corresponding to that model by running the CAMB code [49];
3. generate a map in Healpix [50] consistent with the model;
4. apply the kp0 mask;
5. degrade to NSIDE=32 resolution, then reapply the kp0 mask also degraded to NSIDE=32; and

TABLE VII: Values of $S_{1/2}$ and S_{full} statistics, and their ranks (in percent) relative to Monte Carlo realizations of isotropic skies consistent with best-fit Λ CDM models from WMAP 3 year constraints. All of the maps were subjected to the kp0 mask and compared to 20,000 Monte Carlo realizations with the kp0 mask also applied. The third and second-to-last row are without the mask and compared to 1000 full-sky simulations, while the last row shows the Λ CDM expectation. The boldfaced entries show the extremely small values of $S_{1/2}$ statistic for the 3-year cut-sky maps, while the single italic entry shows that the full-sky ILC123 map does *not* have an unusually small $\mathcal{C}(\theta)$. We also show the quadrupole, octopole and hexadecapole power \mathcal{C}_ℓ estimated from the corresponding $\mathcal{C}(\theta)$; note again the difference between the cut-sky and full-sky values.

Map	$S_{1/2}$ (μK) ²	$P(S_{1/2})$ (%)	S_{full} (μK) ²	$P(S_{\text{full}})$ (%)	$6\mathcal{C}_2/(2\pi)$ (μK) ²	$12\mathcal{C}_3/(2\pi)$ (μK) ²	$20\mathcal{C}_4/(2\pi)$ (μK) ²
Q123	956	0.04	33399	1.91	178	430	799
V123	1306	0.12	27816	0.96	47	403	818
W123	1374	0.14	29706	1.27	35	449	828
Q1	10471	10.2	41499	4.3	79	357	745
V1	2117	0.38	29170	1.16	53	369	796
W1	2545	0.64	30872	1.38	40	405	815
ILC123(cut)	928	0.03	28141	1.04	113	414	831
ILC1(cut)	1172	0.09	29873	1.25	115	443	901
ILC123(full)	8328	<i>7.0</i>	60806	9.1	247	1046	751
ILC1(full)	9119	8.3	70299	14.4	195	1050	828
Λ CDM	39700	—	133000	—	1091	1020	958

- compute $\mathcal{C}(\theta)$ directly from the map, using the unmasked pixels.

In addition, and using the same procedure but without masking, we compute $\mathcal{C}(\theta)$ from 1000 simulated full-sky maps for comparison to full-sky ILC maps. (Since $P(S_{1/2})$ and $P(S_{\text{full}})$ for the full-sky maps are not as low as for the cut-sky maps, we did not need to go through the resource-consuming task of generating 20 times more simulations in order to get good statistics.) We have checked that applying the inverse-noise weighting to the pixels when degrading the map resolution (O. Doré, private communication) leads to negligible differences in the recovered $\mathcal{C}(\theta)$ ($\lesssim 1\mu K^2$ on large scales). Finally we have checked that, for the cut-sky case, applying the kp2 mask instead of kp0 gives similar results.

Results from the comparisons are given in the third and fifth column of Table VII. They indicate that only 0.04%-0.14% of isotropic Λ CDM skies (for the Q, V and W band maps) give $S_{1/2}$ that is smaller than that from WMAP123. Similarly, the masked ILC123 map has $S_{1/2}$ low at the 0.03% level. Interestingly, even the S_{full} statistic that includes power on all scales, applied to cut-sky maps, is low at about a 1% level. We therefore conclude that *the absence of large angle correlations at scales greater than 60 degrees is, at > 99.85% C.L., even more significant in year 123 than in year 1.*

We also show the quadrupole, octopole and hexadecapole power inferred from $\mathcal{C}(\theta)$ of various maps, as well as the Λ CDM expected values. It is clear that the quadrupole and octopole computed from cut-sky $\mathcal{C}(\theta)$ are a factor of two to five smaller than those from the full-sky maps (and of course the latter are another factor of two to four smaller than the most likely Λ CDM values). This result has been hinted at by the WMAP team [12] who

pointed out that the MLE estimates of the quadrupole and octopole (as well as $\ell = 7$) they adopted in year 123 are considerably larger than the pseudo- \mathcal{C}_ℓ values they had adopted in year 1. Here we find that the pseudo- \mathcal{C}_ℓ estimates are in a much better agreement with the cut-sky $\mathcal{C}(\theta)$ than the MLE values; see Figure 5.

The current situation seems to us very disturbing. Standard procedures for extracting the “angular power spectrum” of the CMB uses pseudo- \mathcal{C}_ℓ . The recent WMAP analysis included a maximum-likelihood analysis at low ℓ (described above) to correct for the effects of a cut sky and to mitigate any remaining galaxy contamination. But both the connection between pseudo- \mathcal{C}_ℓ and any properties of the underlying ensemble (whatever that may mean), and the validity of the maximum-likelihood analysis rely on the assumption that the underlying sky (i.e. the ensemble) is statistically isotropic. However, we (and others) have already provided strong evidence that the underlying sky, or at least the all-sky maps, are *not* statistically isotropic. In the absence of statistical isotropy none of the computable quantities have any clear connection to the statistical properties of the underlying ensemble. Indeed, in the absence of statistical isotropy each $a_{\ell m}$ could have its own distinct distribution. Since we have precisely one sample from each such distribution – the value of $a_{\ell m}$ on the actual sky (and even that only for a measured full sky) – it is impossible to in any way characterize these distributions from the observation of just one universe.

We are faced with two choices: either the universe is not statistically isotropic on large scales (perhaps because it has non-trivial topology), or the observed violation of statistical isotropy is not cosmological, but rather due either to systematic errors, or to unanticipated fore-

grounds. In this latter case, it is imperative to get to the root of the problems at large angles.

The disagreement between the full-sky and cut-sky angular correlation functions, evident in Figure 5 and Table VII, is both marked and troubling. The third and second-to-last columns of Table VII show that both the quadrupole and the octopole power estimated from the cut-sky maps are much smaller than those estimated from reconstructed full-sky ILC maps – for each multipole, the former is about one half as large as the latter. However, it is the full-sky values which correspond to the estimated values used in cosmological parameter analyses.

It is of utmost concern to us that one begins with individual band maps that all show very little angular correlation at large angles (i.e. $|\mathcal{C}(\theta)|$ is small), and, as a result of the analysis procedure, one is led to conclude that the underlying cosmological correlations are much larger. What is even more disturbing is that the full-sky map making algorithm is inserting significant extra large angle power into precisely those portions of the sky where we have the least reliable information. We are similarly concerned that the “galactic bias correction” of the ILC123, which inserts extra low- ℓ power into the region of the galactic cut, does so on the basis of the expectations of a model whose assumptions (statistical isotropy and the particular Λ CDM power spectrum) are not borne out even after all the corrections are made. But even the first-year ILC, which did not have this bias correction, suffers from a surfeit of power inside the cut.

Finally, although the maximum likelihood estimates of the low- ℓ C_ℓ (actually \mathcal{C}_ℓ) quoted by WMAP in their three-year release appear to be in better agreement with the Λ CDM model than are the values one derives from cut-sky individual bands, or the cut sky ILC123, or the values quoted in the one-year WMAP release, nevertheless, the angular correlation function that the new quoted C_ℓ imply (as shown in Figure 5) appears to be in even worse agreement with the Λ CDM prediction than all the others.

IV. CONCLUSIONS

We have shown that the ILC123 map, a full sky map derived from the first three years of WMAP data like its predecessors the ILC1, TOH1 and LILC1 maps, derived from the first year of WMAP data, shows statistically significant deviations from the expected Gaussian-random, statistically isotropic sky with a generic inflationary spectrum of perturbations. In particular: there is a dramatic lack of angular correlations at angles greater than sixty degrees; the octopole is quite planar with the three octopole planes aligning with the quadrupole plane; these planes are perpendicular to the ecliptic plane (albeit at reduced significance than in the first-year full-sky maps); the ecliptic plane neatly separates two extrema of the combined $\ell = 2$ and $\ell = 3$ map, with the strongest extrema to the south of the ecliptic and the weaker ex-

trema to the north. The probability that each of these would happen by chance are 0.03% (quoting the cut-sky ILC123 $S_{1/2}$ probability), 0.4%, 10%, and $< 5\%$. As they are all independent and all involve primarily the quadrupole and octopole, they represent a $\sim 10^{-8}$ probability chance “fluke” in the two largest scale modes. To quote [7]: *We find it hard to believe that these correlations are just statistical fluctuations around standard inflationary cosmology’s prediction of statistically isotropic Gaussian random $a_{\ell m}$ [with a nearly scale-free primordial spectrum].*

What are the consequences and possible explanations of these correlations? There are several options — they are statistical flukes, they are cosmological in origin, they are due to improper subtraction of known foregrounds, they are due to a previously unexpected foreground, or they are due to WMAP systematics. As remarked above it is difficult for us to accept the occurrence of a 10^{-8} unlikely event as a scientific explanation.

A cosmological mechanism could possibly explain the weakness of large angle correlations, and the alignment of the quadrupole and octopole to each other. A cosmological explanation must ignore the observed correlations to the solar system, as there is no chance that the universe knows about the orientation of the solar system nor vice-versa. These latter correlations are unlikely at the level of less than 1 in 200 (plus an additional independent $\approx 1/10$ unlikely correlation with the dipole which we have ignored). This possibility seems to us contrived and suggests to us that explanations which do not account for the connection to solar system geometry should be viewed with considerable skepticism.

In [16], we showed that the known Galactic foregrounds possess a multipole vector structure wholly dissimilar to those of the observed quadrupole and octopole. This argues strongly against any explanation of the observed quadrupole and octopole in terms of these known Galactic foregrounds.

A number of authors have attempted to explain the observed quadrupole-octopole correlations in terms of a new foreground [51–56]. (Some of these also attempted to explain the absence of large angle correlations, for which there are also other proffered explanations [57–63].) Only one of the proposals ([53]) can possibly explain the ecliptic correlations, as all the others are extragalactic. Some do claim to explain the less-significant dipole correlations. Difficulties with individual mechanisms have been discussed by several authors [56, 64–67] (sometimes before the corresponding proposal). Unfortunately, in each and every case, among possible other deficiencies, the pattern of fluctuations proposed is inconsistent with the one observed on the sky. As remarked above, the quadrupole of the sky is nearly pure Y_{22} in the frame where the z -axis is parallel to $\hat{w}^{(2,1,2)}$ (or any nearly equivalent direction), while the octopole is dominantly Y_{33} in the same frame. Mechanisms which produce an alteration of the microwave signal from a relatively small patch of sky — and all of the above proposals fall into this

class — are most likely to produce aligned Y_{20} and Y_{30} . (This is because if there is only one preferred direction, then the multipole vectors of the affected multipoles will all be parallel to each other, leading to a Y_{l0} .) The authors of [55] manage to ameliorate the situation slightly by constructing a distorted patch, leading to an underpowered Y_{33} , but still a pure Y_{20} . The second shortcoming of all explanations where contaminating effect is effectively *added* on top of intrinsic CMB temperature is that chance cancellation is typically required to produce the low power at large scales, or else the intrinsic CMB happens to have *even less* power than what we observe. Likelihood therefore disfavors all additive explanations [56] (unless the explanation helps significantly with some aspect of structure seen at higher ℓ).

Explaining the observed correlations in terms of foregrounds is difficult. The combined quadrupole and octopole map suggests a foreground source which form a plane perpendicular to the ecliptic. It is clear neither how to form such a plane, nor how it could have escaped detection by other means. This planar configuration means that single anomalous hot or cold spots do not provide an adequate explanation for the observed effects.

The final possibility is that systematic effects remain in the analysis of the WMAP data. Two systematic corrections have already been introduced between the one-year and the three-year data releases: the improved radiometer gain model, which includes effects correlated with the ecliptic and with the seasons (and hence the equinoxes); and the galaxy bias correction to the ILC. We have discussed the roles of both of these in reducing somewhat the statistical significance of the orthogonality of the quadrupole and octopole planes to the ecliptic. But other systematic effects may remain. For example, a suggestion has been made [8] that observed north-south power asymmetries [9] could be caused by a small error (within the 1σ error bars) in the solar velocity with respect to the CMB. However, this would not explain the correlations in full sky maps noted in this paper [68]. Other possibilities have been put forward, for example a correlation between the scanning pattern and the beam asymmetry [69], but have not been carefully evaluated.

If indeed the observed $\ell = 2$ and 3 CMB fluctuations are not cosmological, there are important consequences. Certainly, one must reconsider [7] all CMB results that rely on low ℓ s, such as the normalization, A , of the primordial fluctuations and any constraint on the running $dn_s/d\log k$ of the spectral index of scalar perturbations (which, as noted in [70], depended in WMAP1 on the absence of low- ℓ TT power). Moreover, the CMB-galaxy cross-correlation, which has been used to provide evidence for the Integrated Sachs-Wolfe effect and hence the existence of dark energy, also gets contributions from the lowest multipoles (though the main contribution comes from slightly smaller scales, $\ell \sim 10$). Finally, note that, even though we have discussed only alignments at $\ell = 2$ and 3, it is possible — even likely — that the underlying physical mechanism does not cut off abruptly at the

octopole, but rather affects $\ell = 4, 5, \dots$. Indeed, several pieces of evidence, though less statistically convincing than those discussed here, have been presented for anomalies at $l > 3$. If the values of C_ℓ for $\ell > 3$ are called into doubt, then so are the values of further cosmological parameters, including the optical depth to the last scattering surface τ , the inferred redshift of reionization, and the rms mass fluctuation amplitude σ_8 .

Of even more fundamental long-term importance to cosmology, a non-cosmological origin for the currently-observed low- ℓ microwave background fluctuations is likely to imply further-reduced correlation at large angles in the true CMB. As shown in Section 3, angular correlations are already suppressed compared to Λ CDM at scales greater than 60 degrees at between 99.85% and 99.97% C.L. (with the latter value being the one appropriate to the cut sky ILC123). This result is *more* significant in the year 123 data than in the year 1 data. *The less correlation there is at large angles, the poorer the agreement of the observations with the predictions of generic inflation. This implies, with increasing confidence, that either we must adopt an even more contrived model of our cosmological conundrums.* Moreover, any analysis of the likelihood of the observed “low- ℓ anomaly” that relies only on the (low) value of C_2 (especially the MLE-inferred) should be questioned. According to inflation C_2 , C_3 and C_4 should be independent variables, but the vanishing of $\mathcal{C}(\theta)$ at large angles suggests that the different low- ℓ C_ℓ are not independent.

Another striking fact seen in Table VII is that the quadrupole and octopole of cut-sky maps, as well as $S_{1/2}$ statistics, are significantly lower than in the full-sky ILC maps, both for year 1 and year 123. This seems to be because of a combination of effects — the “galactic bias correction” and the time-dependent radiometer gain model certainly, but perhaps also just the minimal variance procedure used to build the ILC. This reflects the fact that the synthesized full sky maps show correlations at large angles that are simply not found in the underlying band maps. This does not seem reasonable to us — that one starts with data that has very low correlations at large angles, synthesizes that data, corrects for systematics and foregrounds and then concludes that the underlying cosmological data is much more correlated than the observations — in other words that there is a conspiracy of systematics and foreground to cancel the true cosmological correlations.

This strongly suggests to us that there remain serious issues relating to the failure of statistical isotropy that are permeating the map making, as well as the extraction of low- ℓ C_ℓ .

At the moment it is difficult to construct a single coherent narrative of the low ℓ microwave background observations. What is clear is that, despite the work that remains to be done understanding the origin of the observed statistically anisotropic microwave fluctuations, there are problems looming at large angles for standard

inflationary cosmology.

The authors thank M. Dennis, O. Doré, P. Ferreira, P. Freeman, C. Gordon, G. Hinshaw, W. Hu, K. Inoue, S. Meyer, R. Nichol, H. Peiris, J. Silk, D. Spergel, and R. Trotta for useful discussions. The work of CJC and GDS has been supported by the US DoE and NASA. GDS has also been supported by the John Simon Guggenheim Memorial Foundation and by a fellowship from the Beecroft Centre for Particle Astro-

physics and Cosmology. DH is supported by the NSF Astronomy and Astrophysics Postdoctoral Fellowship under Grant No. 0401066. GDS acknowledges Maplesoft for the use of Maple. We have benefited from using the publicly available CAMB [49] and Healpix [50] packages. We acknowledge the use of the Legacy Archive for Microwave Background Data Analysis (LAMBDA). Support for LAMBDA is provided by the NASA Office of Space Science.

-
- [1] C. L. Bennett *et al.*, *Astrophys. J.* **148**, S1 (2003), astro-ph/0302207.
 - [2] C. L. Bennett *et al.*, *Astrophys. J.* **148**, S97 (2003), astro-ph/0302208.
 - [3] G. Hinshaw *et al.*, *Astrophys. J.* **148**, S135 (2003), astro-ph/0302217.
 - [4] A. Kogut *et al.*, *Astrophys. J.* **148**, S161 (2003), astro-ph/0302213.
 - [5] D. N. Spergel *et al.*, *Astrophys. J.* **148**, S175 (2003), astro-ph/0302209. F. K. Hansen, P. Cabella, D. Marinucci, and N. Vittorio, *Astrophys. J.* **607**, L67 (2004), astro-ph/0402396. F. K. Hansen, A.J. Banday and K.M. Gorski, astro-ph/0404206.
 - [6] A. de Oliveira-Costa, M. Tegmark, M. Zaldarriaga and A. Hamilton, *Phys. Rev. D* **69**, 063516 (2004), astro-ph/0307282.
 - [7] D. J. Schwarz, G. D. Starkman, D. Huterer, and C. J. Copi, *Phys. Rev. Lett.* **93**, 221301 (2004), astro-ph/0403353.
 - [8] P. E. Freeman, C. R. Genovese, C. J. Miller, R. C. Nichol, and L. Wasserman, *Astrophys. J.* **638**, 1 (2006), astro-ph/0510406.
 - [9] H. K. Eriksen, F. K. Hansen, A. J. Banday, K. M. Gorski, and P. B. Lilje, *Astrophys. J.* **605**, 14 (2004); **609**, 1198 (2004) [Erratum], astro-ph/0307507;
 - [10] O. Dore, G. P. Holder, and A. Loeb, *Astrophys. J.* **612**, 81 (2004), astro-ph/0309281.
 - [11] N. Jarosik, *et al.*, astro-ph/0603452.
 - [12] G. Hinshaw, *et al.*, astro-ph/0603451.
 - [13] L. Page, *et al.*, astro-ph/0603450.
 - [14] D. N. Spergel *et al.*, astro-ph/0603449.
 - [15] A. de Oliveira-Costa and M. Tegmark, astro-ph/0603369.
 - [16] C. J. Copi, D. Huterer, D. J. Schwarz, and G. D. Starkman, *Mon. Not. Roy. Astron. Soc.* **367**, 79 (2006), astro-ph/0508047.
 - [17] G. Hinshaw *et al.*, *Astrophys. J.* **464**, L25 (1996), astro-ph/9601061.
 - [18] C. J. Copi, D. Huterer, and G. D. Starkman, *Phys. Rev. D* **70**, 043515 (2004), astro-ph/0310511.
 - [19] M. Limon, *et al.*, “Explanatory Supplement”, 2006
 - [20] The WMAP1 ILC1 map is available at: http://cmbdata.gsfc.nasa.gov/product/map/m_products.cfm
 - [21] M. Tegmark, A. de Oliveira-Costa and A. J. S. Hamilton, *Phys. Rev. D* **68**, 123523 (2003), astro-ph/0302496.
 - [22] H. K. Eriksen, A. J. Banday, K. M. Gorski, and P. B. Lilje, *Astrophys. J.* **612**, 633 (2004), astro-ph/0403098.
 - [23] L. Y. Chiang, P. D. Naselsky, O. V. Verkhodanov and M. J. Way, *Astrophys. J.* **590**, L65 (2003), astro-ph/0303643; P. Naselsky, L. Y. Chiang, P. Olesen and I. Novikov, *Phys. Rev. D* **72**, 063512 (2005), astro-ph/0505011.
 - [24] C.-G. Park, *Mon. Not. Roy. Astron. Soc.* **349**, 313 (2004), astro-ph/0307469.
 - [25] P. Vielva, E. Martinez-Gonzalez, R. B. Barreiro, J. L. Sanz, and L. Cayon, *Astrophys. J.* **609**, 22 (2004), astro-ph/0310273; M. Cruz, E. Martinez-Gonzalez, P. Vielva and L. Cayon, *Mon. Not. Roy. Astron. Soc.* **356**, 29 (2005), astro-ph/0405341; M. Cruz, M. Tucci, E. Martinez-Gonzalez and P. Vielva, astro-ph/0601427; Y. Wiaux, P. Vielva, E. Martinez-Gonzalez and P. Vanderghenst, *Phys. Rev. Lett.* **96**, 151303 (2006), astro-ph/0603367.
 - [26] J. P. Ralston and P. Jain, *Int. J. Mod. Phys. D* **13**, 1857 (2004), astro-ph/0311430.
 - [27] V. G. Gurzadyan *et al.*, *Nuovo Cim.* **118B**, 1101 (2003), astro-ph/0402399; V. G. Gurzadyan *et al.*, *Mod. Phys. Lett. A* **20**, 491 (2005), astro-ph/0312305.
 - [28] J.D. McEwen, M.P. Hobson, A.N. Lasenby and D.J. Mortlock, *Mon. Not. Roy. Astron. Soc.* **359**, 1583 (2005), astro-ph/0406604.
 - [29] P. Mukherjee and Y. Wang, *Astrophys. J.* **613**, 51 (2004), astro-ph/0402602.
 - [30] E.P. Donoghue and J.F. Donoghue, *Phys. Rev. D* **71**, 043002 (2005), astro-ph/0411237.
 - [31] P. Bielewicz, K.M. Gorski, and A.J. Banday, *Mon. Not. Roy. Astron. Soc.* **355**, 1283 (2004), astro-ph/0405007
 - [32] K. Land and J. Magueijo, *Mon. Not. Roy. Astron. Soc.*, **357**, 994 (2005), astro-ph/0405519.
 - [33] K. Land and J. Magueijo, *Mon. Not. Roy. Astron. Soc.* **362**, L16 (2005), astro-ph/0407081; *Phys. Rev. Lett.* **95**, 071301 (2005), astro-ph/0502237; *Mon. Not. Roy. Astron. Soc.* **362**, 838 (2005), astro-ph/0502574.
 - [34] K. Land and J. Magueijo, *Phys. Rev. D* **72**, 101302 (2005), astro-ph/0507289.
 - [35] A. Bernui *et al.*, astro-ph/0601593
 - [36] A. Hajian, T. Souradeep and N.J. Cornish, *Astrophys. J.* **628**, L63 (2004), astro-ph/0406354; A. Hajian and T. Souradeep, astro-ph/0501001.
 - [37] C. Armendariz-Picon, astro-ph/0509893.
 - [38] J. Medeiros and C.R. Contaldi, *Mon. Not. Roy. Astron. Soc.* **367**, 39 (2006), astro-ph/0510816.
 - [39] L. Y. Chiang, P. D. Naselsky and P. Coles, astro-ph/0603662
 - [40] J. C. Maxwell, *A Treatise on Electricity and Magnetism*, Vol I, 3rd edition, Clarendon Press, London, 1891.
 - [41] M. R. Dennis, *J. Phys. A: Math. Gen.* **37**, 9487 (2004).
 - [42] J.R. Weeks, astro-ph/0412231.

- [43] G. Katz G. and J. Weeks, Phys. Rev. **D70**, 063527 (2004), astro-ph/0405631.
- [44] A. Slosar and U. Seljak, Phys. Rev. **D70**, 083002 (2004), astro-ph/0404567.
- [45] P. Bielewicz, H.K. Eriksen, A.J. Banday, K.M. Górski and P.B. Lilje, Astrophys. J. **635**, 750 (2005), astro-ph/0507186
- [46] L. R. Abramo et al., astro-ph/0604346.
- [47] R.C. Helling, P. Schupp and T. Tesileanu, astro-ph/0603594.
- [48] A. Slosar, U. Seljak and A. Makarov, Astrophys. J., submitted, astro-ph/0403073
- [49] A. Lewis, A. Challinor and A. Lasenby, Astrophys. J. **538**, 473 (2000), astro-ph/9911177
- [50] K. Gorski, E. Hivon, A.J. Banday, B. D. Wandelt, F.K. Hansen, M. Reinecke and M. Bartelmann, Astrophys. J. **622**, 759 (2005), astro-ph/0409513; K. Gorski, E. Hivon, and B. D. Wandelt, Proceedings of the MPA/ESO Cosmology Conference “Evolution of Large-Scale Structure”, eds. A. J. Banday, R. S. Sheth and L. Da Costa, PrintPartners Ipskamp, NL, pp. 37-42 (astro-ph/9812350); <http://www.eso.org/science/healpix/>.
- [51] T. Ghosh, A. Hajian and T. Souradeep, astro-ph/0604279.
- [52] J. W. Moffat, JCAP **0510**, 012 (2005), astro-ph/0502110.
- [53] P. C. Frisch, Astrophys. J. **632**, L143 (2005), astro-ph/0506293.
- [54] C. Vale, astro-ph/0509039.
- [55] K. T. Inoue and J. Silk, astro-ph/0602478.
- [56] C. Gordon, W. Hu, D. Huterer and T. Crawford, Phys. Rev. D **72**, 103002 (2005), astro-ph/0509301.
- [57] J.M. Cline, P. Crotty and J. Lesgourgues, JCAP **0309**, 010 (2003), astro-ph/0304558.
- [58] C. R. Contaldi, M. Peloso, L. Kofman and A. Linde, JCAP **0307**, 002 (2003), astro-ph/0303636.
- [59] J. P. Luminet, J. Weeks, A. Riazuelo, R. Lehoucq and J. P. Uzan, Nature **425**, 593 (2003), astro-ph/0310253.
- [60] A. Niarchou, A.H. Jaffe and L. Pogosian, Phys. Rev. D **69**, 063515 (2004),
- [61] J. Weeks, J. P. Luminet, A. Riazuelo and R. Lehoucq, Mon. Not. Roy. Astron. Soc. **352**, 258 (2004), astro-ph/0312312.
- [62] L. R. Abramo and L. J. Sodre, astro-ph/0312124.
- [63] C. Gordon and W. Hu, Phys. Rev. D **70**, 083003 (2004), astro-ph/0406496.
- [64] F. Ferrer, S. Räsänen, and J. Valiviita, JCAP **0410**, 010 (2004), astro-ph/0407300.
- [65] A. Rakić, S. Räsänen and D. J. Schwarz, Mon. Not. Roy. Astron. Soc. (submitted), astro-ph/0601445.
- [66] F. K. Hansen, E. Branchini, P. Mazzotta, P. Cabella and K. Dolag, Mon. Not. Roy. Astron. Soc. **361**, 753 (2005), astro-ph/0502227.
- [67] A. Cooray and N. Seto, JCAP **0512**, 004 (2005), astro-ph/0510137.
- [68] P. Freeman, private communication.
- [69] S. Meyer, private communication.
- [70] R. Rebolo, *et al.*, Mon. Not. R. Astron. Soc., **353**, 747 (2004), astro-ph/0402466.